07,09,13

The Effect of Heat Treatment on the Thermal Conductivity of Single Crystals of Solid Solutions Based on ZrO_2 Stabilized by Scandium, Cerium, and Yttrium Oxides

© D.A. Agarkov[1], M.A. Borik[2], E.V. Vakulina[4], E.V. Ezhikova[2], A.V. Kulebyakin[2], E.E. Lomonova[2], F.O. Milovich[3], V.A. Myzina[2], P.A. Popov[4], A.A. Reu[2], P.A. Ryabochkina[5], N.Yu. Tabachkova[2,3], A.S. Chislov[2,3]

[1] Osipyan Institute of Solid State Physics of RAS, Chernogolovka, Russia
[2] Prokhorov General Physics Institute of RAS, Moscow, Russia
[3] Department of Materials Science of Semiconductors and Dielectrics, National University of Science and Technology „MISIS“, Moscow, Russia
[4] Petrovsky Bryansk State University, Bryansk, Russia
[5] Ogarev Mordovia State University, Saransk, Russia

E-mail: chislov.as@misis.ru

Received January 13, 2026
Revised February 5, 2026
Accepted February 5, 2026

The effect of heat treatment at 1000 °C for 400 h on thermal conductivity of zirconium dioxide crystals co-doped with scandium and cerium oxides, as well as additionally doped with yttrium oxide, has been studied. It was demonstrated that crystal annealing, depending on composition, resulted in phase and structural changes associated with the ordering of oxygen vacancies, which impacted the thermal conductivity in the temperature range 50−300 K. The introduction of Y_2O_3 into the composition of stabilizing additives increased the phase and structural stability of crystals. With the rise of total concentration of doping impurities the effect of annealing on thermal conductivity was noticed to decline.

Keywords: zirconium dioxide, structure, annealing, physicochemical properties.

DOI: 10.61011/PSS.2026.02.63387.8970

1. Introduction

Zirconium dioxide-based materials are widely used in high-temperature engineering as thermal barriers, protective coatings, structural materials, and solid electrolytes [1–6]. The operation of materials at elevated temperatures and in oxidizing media requires not only knowledge of their thermal-physical characteristics, but also an estimate of their stability under prolonged high-temperature exposure.

Zirconium dioxide has three polymorphic modifications: monoclinic, tetragonal and cubic. To prevent phase transitions, oxides of alkaline earth and rare earth elements (REE) are usually introduced into ZrO_2, including Y_2O_3 and Sc_2O_3 [7–9]. The resulting solid solutions, depending on the type and concentration of stabilizing additives, may have different crystal structures and undergo phase transitions in different temperature ranges. As can be seen from the state diagrams, in $ZrO_2-R_2O_3$ system (R = REE, Y, Sc) there are various polymorphic modifications of solid solutions, such as monoclinic, tetragonal, cubic, rhombohedral, characteristic of the range concentrations of introduced impurities from 0 to 40 mol.% R_2O_3 [10–19]. The boundaries of their existence are determined by the type of a doping impurity. So far, the state diagrams for $ZrO_2-R_2O_3$ system have been studied in the most detail, although even in this system, the phase boundaries may differ according to a number of authors [12]. In synthesis of materials with their compositions approaching the phase interface, the structure of a material may vary greatly depending on the fabrication method and synthesis conditions. The most complex diagram of state with significant uncertainty of the phase boundaries positions and narrow phase existence regions, as noted in the literature, is peculiar to the system $ZrO_2-Sc_2O_3$ [18,19]. Therefore, the structure of materials containing Sc_2O_3 in solid solutions is most sensitive to the conditions of their fabrication.

In recent years, zirconium dioxide-based materials doped with several oxides have attracted considerable interest. Co-doping, as a rule, is aimed at modifying physico-chemical (including thermal-physical) properties and increasing phase stability under high-temperature exposure. It is shown that co-doping with oxides of rare earth elements makes it possi-

ble not only to improve the thermal insulation characteristics of yttrium-stabilized zirconium dioxide (YSZ), but also to increase its heat resistance [20–23]. At the same time, the systematized data on the phase diagrams of ternary systems remain limited [14–16], which makes it difficult to predict the phase evolution and degradation of properties during long heat treatment. Despite a large number of studies highlighting the stability of ZrO_2 solid solutions and degradation of their physico-chemical characteristics [24–32], the effect of heat treatment on thermal-physical properties (in particular, thermal conductivity) has been reviewed only in a limited number of publications.

Thermal conductivity is very sensitive to the material structural specifics, such as oxygen vacancies, impurity cations, complexes of vacancies and solid solution cations, and locally ordered structures. In the study of zirconium dioxide doped with several impurities, it was observed that numerous oxygen vacancies and lattice distortion, a change in the coordination number of Zr^{4+} cations and the rise of potential energy of tetragonal phase conversion into monoclinic phase contributed to higher phase stability of the tetragonal phase and maintaining high mechanical characteristics at higher temperatures [33–37]. Oxygen vacancies, impurity cations, their complexes, and lattice distortions are sources of phonon scattering; thus, these structural defects contribute to a decrease in the thermal conductivity of the material [22,36]. Today, a slew of papers give an insight into the process of doping of zirconium dioxide stabilized with yttrium oxide, Sc_2O_3 [29,37,38] and CeO_2 oxides [39–41], as well as into co-doping of the material with these oxides [36]. As mentioned in the literature, when YSZ is co-doped with cerium and scandium oxides, the ceramic material CeScYSZ has the lowest thermal conductivity ($1.53\,W/(m\cdot K)$) and phase stability at 1500 °C for a long time [36]. The combination of low thermal conductivity with good mechanical characteristics makes such ceramics promising materials for thermal barrier coatings.

The thermal-physical properties of zirconium dioxide-based materials have been studied mainly on ceramic materials. Dense ceramics are used to study the temperature dependences of thermal conductivity. If it is necessary to reduce the thermal conductivity, some process methods are used in synthesis aimed at forming the microstructure specifics of the material, such as grain size, porosity, type of structure, etc. It should be stressed that the use of single crystal specimens to study the effect of the material's structure specifics on the amount of thermal conductivity allows to neglect the effect of grain boundaries, presence of pores and other singularities, inherent in polycrystalline ceramic materials, depending on the synthesis method. The study of single crystals allows identifying the dependence of thermal-physical characteristics on the material composition, in particular on composition of a solid solution based on zirconium dioxide.

Previously, we examined thermal conductivity of single crystals of ZrO_2 solid solutions, doped with scandium, cerium, and yttrium oxides [41]. Single crystals with a total content of the doping impurities of scandium, cerium, and yttrium from 9 to 11.5 mol.% were studied. Scandium oxide content was from 8 to 10 mol.%, cerium oxide content — from 0.5 to 1 mol.%, yttrium oxide — from 0.5 to 2 mol.%. In this regard, the greatest influence on thermal conductivity was exerted by the concentration of Sc_2O_3, an increase in which contributed to lower thermal conductivity of crystals. The obtained results show that a change in the concentration ratio of doping impurities led to a change in the phase composition and, accordingly, the structure of the solid solution, which affected its thermal conductivity. Higher number of defects in the fluorite structure in crystals is explained by the following: the presence of a twin structure characteristic of tetragonal and rhombohedral phases; the content of several phases in the crystal or regions with a local ordering of oxygen vacancies; and the change in the amount of zirconium cations with a coordination number less than 8. This helps to reduce the thermal conductivity of zirconium dioxide based solid solutions.

The purpose of this work was to study the phase stability of solid solutions $(ZrO_2)_{1-x-y}(Sc_2O_3)_x(CeO_2)_y$, where $x = 0.08-0.1$; $y = 0.005-0.01$ and $(ZrO_2)_{1-x-y-z}(Sc_2O_3)_x(CeO_2)_y(Y_2O_3)_z$, where $x = 0.08-0.1$; $y = 0.005-0.01$; $z = 0.005-0.02$, and the impact of thermal treatment 1000 °C for 400 h on their thermal conductivity.

2. Experimental part

Using the method of directional solidification of a melt in a cold container in „Kristall-407" setup the two series of solid solutions crystals based on zirconium dioxide were grown stabilized with scandium and cerium oxides $(ZrO_2)_{1-x-y}(Sc_2O_3)_x(CeO_2)_y$, where $x = 0.08-0.1$; $y = 0.005-0.01$, and simultaneously stabilized with the oxides of scandium, cerium and yttrium $(ZrO_2)_{1-x-y-z}(Sc_2O_3)_x(CeO_2)_y(Y_2O_3)_z$, where $x = 0.08-0.1$; $y = 0.005-0.01$; $z = 0.005-0.02$. Diameter of cold container — 120 mm, frequency of the high-frequency setup 5.28 MHz, working medium — air, solidification rate 10 mm/h. The starting materials were powdered oxides with a purity of at least 99.99 wt.% of the basic substance.

Heat treatment was carried out in air at 1000 °C for 400 h using a Supertherm HT04/16 high-temperature furnace. The same specimens were used for which thermal conductivity had been determined immediately after crystal growth.

The phase analysis was performed by X-ray diffractometry at Bruker D8 setup using CuK_α radiation and Raman scattering spectroscopy (RS). Laser with a wavelength of 532 nm was used as an excitation source.

The microstructure of the crystals was studied by optical microscopy using Discovery V12 stereomicroscope. Optical microscopy was used to study the crystal structure.

Table 1. The composition of the studied crystals, designations and their density before and after annealing

Composition $ZrO_2-R_2O_3-R'_2O_3$, mol.%				Designation	Density, g/cm^3	
ZrO_2	Sc_2O_3	CeO_2	Y_2O_3		after growth	after annealing
91	8.5	0.5	–	8.5Sc0.5CeSZ	5.776 ± 0.002	5.80 ± 0.002
90	9	1	–	9Sc1CeSZ	5.791 ± 0.001	5.789 ± 0.001
90	9.5	0.5	–	9.5Sc0.5CeSZ	5.778 ± 0.001	5.759 ± 0.001
89.5	10	0.5	–	10Sc0.5CeSZ	5.738 ± 0.001	5.706 ± 0.008
89.5	8	0.5	2	8Sc0.5Ce2YSZ	5.829 ± 0.001	5.807 ± 0.005
88.5	9	0.5	2	9Sc0.5Ce2YSZ	5.788 ± 0.002	5.759 ± 0.001
91	8	0.5	0.5	8Sc0.5Ce0.5YSZ	5.829 ± 0.001	5.799 ± 0.014
90	9	0.5	0.5	9Sc0.5Ce0.5YSZ	5.785 ± 0.002	5.742 ± 0.017
89.5	9.5	0.5	0.5	9.5Sc0.5Ce0.5YSZ	5.767 ± 0.001	5.756 ± 0.005

Thermal conductivity of crystals after annealing in the temperature of 50–300 K was determined experimentally by the absolute stationary method of longitudinal heat flow. A description of the experimental setup and measurement procedure was provided in [42]. The error in the absolute value of thermal conductivity did not exceed ±6 %. The specimens in the form of parallelepipeds with dimensions $\sim 7\times7\times(15-20)$ mm were cut from crystals along their growth axis, the direction of the crystallographic orientation was arbitrary. The density was determined by hydrostatic weighing on an electronic scale CE 224-C by „Sartorius".

3. Results and discussion

Table 1 shows the composition, designations, and density before and after annealing of the studied crystal samples.

After annealing all crystals of ScCeSZ and ScCeYSZ changed their color. The crystals colored orange-red became colorless after annealing, while retaining the volumetric light scattering and the corresponding microstructure (Figure 1). The color change is due to a change in the valence state of $Ce^{3+} \rightarrow Ce^{4+}$ during annealing [43–45]. After annealing, regions with a structure more characteristic of the rhombohedral phase appeared in ScCeSZ crystals [42] (Figure 1, *b, d, f–h*). Regions with such a structure were absent in ScCeYSZ crystals after annealing.

Figure 2 shows graphs $k(T)$ of the temperature dependences of ScCeSZ crystals thermal conductivity before and after heat treatment at a temperature of 1000 °C for 400 h; for several temperatures, the values of thermal conductivity are given in Table 2.

A study of thermal conductivity of crystals grown from ScCeSZ melt with a total concentration of co-doping oxides from 9 to 10.5 mol.% showed that the temperature dependence of thermal conductivity $k(T)$ before heat treatment is weak and the values of thermal conductivity (see Table 2) are low, which indicates the presence of significant phonon scattering processes in these crystalline materials [31,36,42,46,47]. It is shown in [41] that with an increase in the concentration of scandium oxide in crystals, a decrease in thermal conductivity occurs due to the substitution of some of Zr^{4+} cations with Sc^{3+} cations. The atomic mass of the scandium cation (44.96 u) is two times less than the mass of zirconium cations (91.22 u). The introduction of Ce^{3+} cations with a higher mass than those of Zr^{4+} and Sc^{3+} (140.12 u) into crystals has a significantly lower effect on thermal conductivity of crystals due to the low concentration of the introduced cerium oxide impurity compared to the scandium oxide concentration.

Crystals are dielectrics with a disordered fluorite structure, where oxygen vacancies, dislocations and structurally ordered regions with the presence of a short-range order occur, the sizes of which are commensurate with atomic ones. Phonon scattering at the boundary of these regions will prevail at different temperatures. In this case, the phonon free path should not depend on temperature. Accordingly, the thermal conductivity coefficient of these dielectrics will be proportional to T^3 at low temperatures and will not depend on T at high temperatures.

After annealing, there are small changes in the nature of the temperature dependence and the magnitude of thermal conductivity, and they depend on the composition of crystals (Figure 2 and Table 2). A noticeable decrease in thermal conductivity for 8.5Sc0.5CeSZ, 9Sc1CeSZ, and 9.5Sc0.5CeSZ crystals was observed in the temperature range of 50–100 K, and in the temperature range of 200–300 K, the values of thermal conductivity before and after annealing become closer. Thus, the steepness of $k(T)$ curves after annealing of 8.5Sc0.5CeSZ, 9Sc1CeSZ, 9.5Sc0.5CeSZ crystals rises. If for 8.5Sc0.5CeSZ, 9Sc1CeSZ crystals the thermal conductivity after annealing at 300 K is practically equal to that before annealing, for 9.5Sc0.5CeSZ specimen thermal conductivity slightly declines (Table 2, Figure 1). Heat treatment of 10Sc0.5CeSZ crystal did not af-

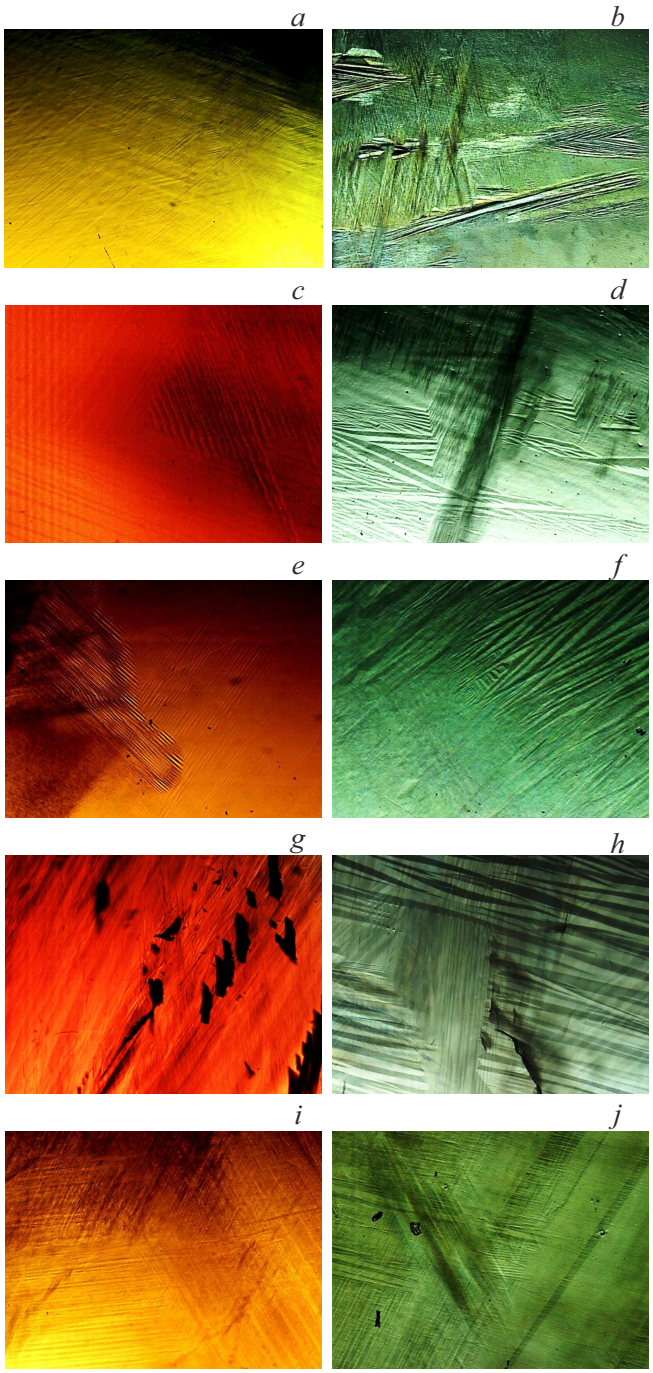

Figure 1. Microstructure in the volume of crystals of solid solutions before and after annealing: 8.5Sc0.5CeSZ — *a*) before annealing, *b*) after annealing; 9Sc1CeSZ — *c*) before annealing, *d*) after annealing; 9.5Sc0.5CeSZ — *e*) before annealing, *f*) — after annealing; 10Sc0.5CeSZ — *g*) before annealing, *h*) after annealing; 8Sc0.5Ce0.5YSZ — *i*) before annealing, *j*) after annealing.

fect the nature of the temperature dependence and the value of thermal conductivity in the studied temperature range.

Changes in thermal conductivity of crystals depend on changes in the local structure of the lattice and phase composition during heat treatment. It was demonstrated [47] that when defects in the lattice are ordered to form regions with a short-range order (defective complexes), the steepness of the thermal conductivity curve becomes larger compared with that for a random distribution of defects. In addition, it was mentioned [47] that the ordering of oxygen vacancies and the formation of a phase with a tetragonal structure during exposure at high temperatures have different effects on thermal conductivity. In contrast to the ordering of oxygen vacancies with the formation of regions of a local structure, the transition to a tetragonal structure can be described as a displacement of oxygen columns. The authors have shown that the structural transformation into the tetragonal phase is a way less effective for phonon scattering, which increases thermal conductivity. This was proved by comparing thermal conductivity of specimen 9.7 mol.% Y_2O_3, measured after synthesis and after annealing at 750 °C for a period of 8 months.

Earlier it was demonstrated [30,48–50], that when cerium oxides $x = 0.08-0.10$, $y = 0.005-0.010$ were introduced into $(ZrO_2)_{1-x}(Sc_2O_3)_y$ crystals no any single-phase cubic crystals could be obtained. The phase composition of crystals before annealing was a mixture of several phases —tetragonal, cubic, and rhombohedral, depending on the concentration of the components of the solid solution. Thus, with an increase in total concentration of co-doping oxides of cerium and scandium by more than 10 mol.% the phase composition of the crystal contained a rhombohedral phase mixed with a cubic one [31,49–50]. The study [30] described the phase stability and transport characteristics of crystals of solid solutions $(ZrO_2)_{1-x-y}(Sc_2O_3)_x(CeO_2)_y$ and $(ZrO_2)_{1-x-y-z}(Sc_2O_3)_x(CeO_2)_y(Y_2O_3)_z$ ($x = 0.08-0.10$; $y = 0.005-0.010$; $z = 0.005-0.02$) after their annealing at a temperature of 1000 °C for 400 h. X-ray diffraction and Raman spectra examinations to determine the phase composition of crystals doped with scandium and cerium have shown that annealing leads to a change in the phase composition. In crystals that previously had only tetragonal and cubic phases, a rhombohedral phase appears. During annealing of 9Sc1CeSZ, 9.5Sc0.5CeSZ crystals, the rhombohedral phase occurs due to a lower concentration of cubic phase, while the content of the tetragonal phase practically does not change [30].

Figure 3 shows the RS spectra of ScCeSZ crystals before and after annealing, which were used to analyze the effect of annealing on thermal conductivity.

It can be seen how RS spectra change after annealing, which indicates changes in the phase composition of crystals. 8.5Sc0.5CeSZ crystals, with their RS spectrum close to that of 9Sc1CeSZ crystals after growth, have a spectrum more characteristic of the tetragonal structure after annealing, where the lines of rhombohedral structure are practically absent. For 9Sc1CeSZ crystals, the RS spectral lines characteristic of the rhombohedral structure are clearly visible in the range 500–607 cm^{-1} [50]. The

Table 2. Thermal conductivity of ScCeSZ single crystal specimens

T, K	k, W/(m · K)									
	8.5Sc0.5CeSZ		9Sc1CeSZ		9.5Sc0.5CeSZ		10Sc0.5CeSZ		10ScSZ	
	growth	annealing	growth	annealing	growth	annealing	growth	annealing	growth	annealing
50	1.41	0.74	1.33	0.69	1.30	0.62	0.48	0.45	0.67	0.69
100	1.53	1.15	1.54	1.23	1.53	1.13	0.94	0.93	1.10	1.11
200	2.00	1.88	2.00	1.92	1.98	1.83	1.70	1.65	1.76	1.77
300	2.32	2.29	2.30	2.33	2.31	2.21	2.05	2.04	2.04	2.06

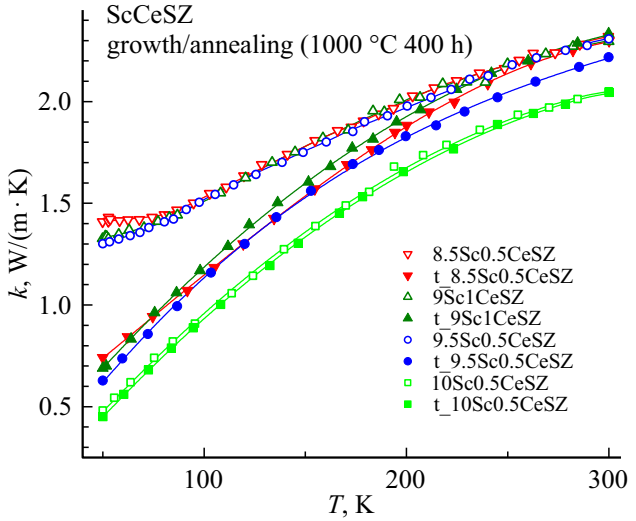

Figure 2. Temperature dependence of thermal conductivity in ScCeSZ crystals: 8.5Sc0.5CeSZ; 9Sc1CeSZ; 9.5Sc0.5CeSZ and 10Sc0.5CeSZ before and after (prefix t_) thermal treatment.

With the same total content of the doping impurities of scandium and cerium oxides in 9Sc1CeSZ and 9.5Sc0.5CeSZ crystals, higher content of scandium oxide and lower content of cerium oxide leads to more significant changes in the phase composition after annealing and, accordingly, in thermal conductivity (Table 2, Figure 2). According to the quantitative analysis of the phase composition by X-ray diffraction [30] method, up to ~ 5 wt.% of the rhombohedral phase appears in 9Sc1CeSZ crystals after annealing due to a decrease in the content of the cubic phase from ~ 15 to 10 wt.%. And for 9.5Sc0.5CeSZ crystals these changes are more essential. The content of the rhombohedral phase in 9.5Sc0.5CeSZ crystals after annealing is up to ~ 15 wt.%, and the content of the cubic phase goes down from ~ 20 to 5 wt.%. Because the rhombohedral phase content after annealing in 9.5Sc0.5CeSZ crystals is higher than in 9Sc1CeSZ crystals the thermal conductivity of 9.5Sc0.5CeSZ crystals declines over the entire temperature range studied, and the thermal conductivity of 9Sc1CeSZ

Raman spectra of 10Sc0.5CeSZ crystals remain virtually unchanged after annealing, indicating that the phase composition, represented by a mixture of rhombohedral and cubic phases, is preserved [50].

Thus, after a prolonged annealing (400 h) at a temperature of 1000 °C, the appearance in solid solutions 8.5Sc0.5CeSZ, 9Sc1CeSZ, 9.5Sc0.5CeSZ of local regions with structures close to the structure of rhombohedral and tetragonal phases as a result of oxygen vacancies ordering causes a decline in thermal conductivity of these crystals at low temperatures and an increase in steepness of the thermal conductivity temperature curve. A more noticeable increase in the rhombohedral phase content in 9.5Sc0.5CeSZ crystals after annealing leads to a lower thermal conductivity at a temperature of 300 K. For 10Sc0.5CeSZ crystals having the lowest thermal conductivity among the studied crystals, the presence of rhombohedral and cubic phases both after growth and after annealing leads to the fact that the thermal conductivity and the nature of its temperature dependence practically do not change after annealing.

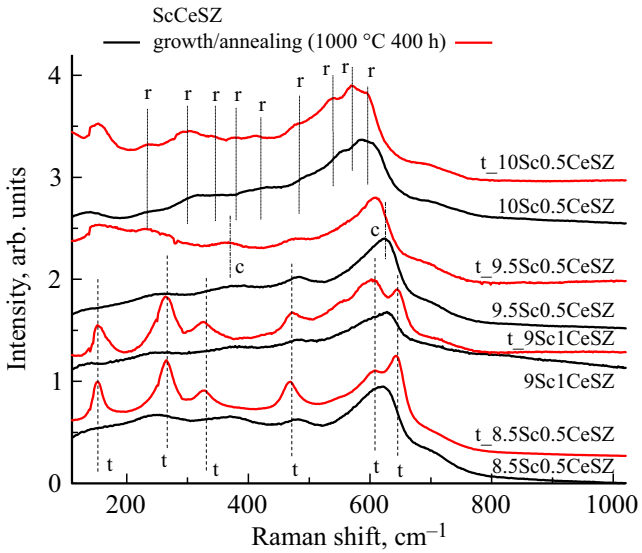

Figure 3. RS spectra of ScCeSZ crystals before and after annealing at a temperature of 1000 °C during 400 h (r — rhombohedral phase, t — tetragonal phase, c — cubic phase).

crystals at temperatures of 200–300 K practically does not change after annealing.

The effect of annealing on crystal density was investigated (Table 1) in ScCeSZ crystals, the addition of scandium oxide (density 3.864 g/cm^3) to zirconium dioxide (density 5.68 g/cm^3) reduces the density of the material, and co-doping with cerium oxide (density 7.65 g/cm^3) leads to its rising. The density value is influenced by the type of the solid solution structure. Among the cubic, rhombohedral, and tetragonal phases present in ScCeSZ crystals, the latter has the highest density. Therefore, the density of 10Sc0.5CeSZ crystals containing cubic and rhombohedral phases is lower than the density of 8.5Sc0.5CeSZ and 9.5Sc0.5CeSZ crystals, the main content of which is the tetragonal phase [31,48–49]. After annealing, the density of 8.5Sc0.5CeSZ crystals remained virtually unchanged, since the crystals retained a predominantly tetragonal phase. For the remaining crystals, the appearance of a rhombohedral phase leads to lower density after annealing. In addition, as a result of annealing, some of cerium cations changed their valence state $Ce^{3+} \rightarrow Ce^{4+}$, which is associated with a change in the ionic radius of the cerium cation and a decrease in the number of oxygen vacancies. This may also lead to changes in density. CeO_2 is characterized by a higher packing density and a higher density than Ce_2O_3. The density values of these oxides are 7.65 and 6.2 g/cm^3 respectively. However, concentration of cerium oxide in crystals is small (0.5 mol.%), and a change in the valence state occurs only for some of its cations [43,44], and therefore density changes after annealing can be considered insignificant.

Figure 4 and Table 3 show the temperature dependences of thermal conductivity of ScCeYSZ crystals before and after heat treatment at a temperature of 1000 °C for 400 h.

As noted in [48–50], additional doping of ScCeSZ crystals with yttrium oxide makes it possible to obtain homogeneous single-phase cubic crystals (8Sc0.5Ce2YSZ, 9Sc0.5Ce2YSZ). Crystals with compositions (8–9.5)Sc0.5Ce0.5YSZ had cubic and tetragonal phases in their composition. The effect of annealing at 1000 °C for 400 h on the phase composition of these crystals and their transport characteristics is analyzed in [30]. It is noted that annealing did not cause fundamental changes in the phase composition of ScCeYSZ crystals. With the exception of specimen 8Sc0.5Ce0.5YSZ, the lattice parameters of the crystal structure remained virtually unchanged after annealing for all crystals. In specimen 8Sc0.5Ce0.5YSZ (total concentration of co-doping oxides is 9 mol.%), the degree of the lattice tetragonal structure increased due to an increase in parameter c and a decrease in parameter a of the tetragonal phase. These changes after annealing are explained by a decrease in the size of cerium ions as a result of transition $Ce^{3+} \rightarrow Ce^{4+}$ and a decrease in the number of vacancies caused by the fact that the replacement of Zr^{4+} ion with Ce^{4+} ion in the lattice does not require charge compensation [30]. In all other crystals with a higher total concentration of stabilizing oxides, the lattice parameters

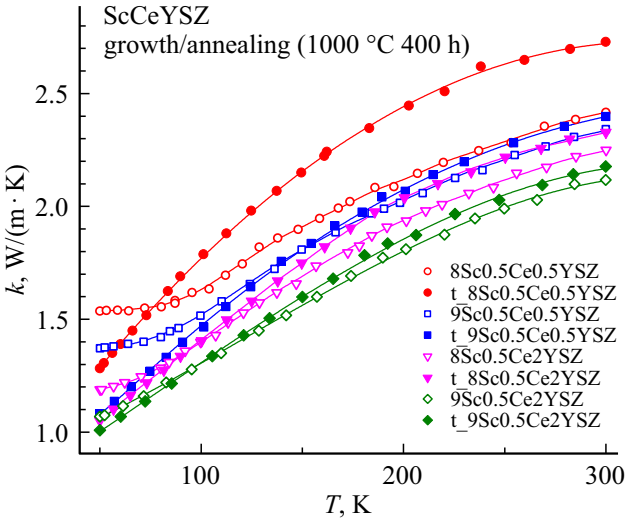

Figure 4. Temperature dependence of thermal conductivity in ScCeYSZ crystals: 8Sc0.5Ce0.5YSZ; 9Sc0.5Ce0.5YSZ; 8Sc0.5Ce2YSZ; 9Sc0.5Ce2YSZ before and after heat treatment.

remained virtually unchanged after annealing. Figure 5 illustrates RS spectra of ScCeYSZ crystals before and after annealing.

After annealing, the intensity of the lines characteristic of the tetragonal phase increased in RS spectrum for almost all ScCeYSZ crystals. These lines are most distinct in RS spectrum of 8Sc0.5Ce0.5YSZ and 9Sc0.5Ce0.5YSZ crystals with a total concentration of the co-doping oxides 9 and 10 mol.%. For 9Sc0.5Ce2YSZ crystal, RS spectrum changed little and remained characteristic of the cubic phase with an additional line of 480cm^{-1}, which indicates the presence of t″ phase close to cubic phase after annealing in the crystals [30]. In contrast to ScCeSZ, in ScCeYSZ crystals no rhombohedral phase appears after annealing.

For crystals of ScCeYSZ, additionally introduced yttrium oxide with a density of 5.016 g/cm^3, lower than that of zirconium dioxide, has less effect on crystal density due to low concentrations compared with the concentration of scandium oxide. The content of scandium and the phase composition of crystals are crucial. After annealing, the crystal density does not change very significantly and it changes to a lesser extent for ScCeSZ crystals (Table 1).

The temperature dependence of thermal conductivity $k(T)$ before and after heat treatment in a series of ScCeYSZ crystals for 9Sc0.5Ce2YSZ remained virtually unchanged over the entire temperature range (Figure 4). The greatest changes in thermal conductivity are observed for 8Sc0.5Ce0.5YSZ crystals, the thermal conductivity of which decreased in the temperature range of 50–70 K and increased in the range of 70–300 K, resulting in a significant change in the temperature dependence of thermal conductivity. These changes are probably related to a noticeable increase in the tetragonal phase in 8Sc0.5Ce0.5YSZ crystal and the ordering of oxygen vacancies. With higher total

Table 3. Thermal conductivity of ScCeYSZ single crystals before and after annealing

T, K	k, W/(m · K)									
	8Sc0.5Ce0.5 YSZ		9Sc0.5Ce0.5 YSZ		9.5Sc0.5Ce0.5 YSZ		8Sc0.5Ce2 YSZ		9Sc0.5Ce2 YSZ	
	growth	annealing	growth	annealing	growth	annealing	growth	annealing	growth	annealing
50	1.54	1.29	1.37	1.08	1.21	1.11	1.19	1.05	1.07	1.00
100	1.63	1.77	1.52	1.47	1.41	1.40	1.40	1.41	1.30	1.31
200	2.12	2.45	2.03	2.08	1.93	1.96	1.93	2.04	1.80	1.86
300	2.42	2.73	2.34	2.40	2.26	2.30	2.25	2.33	2.12	2.17

content of the doping impurity in ScCeYSZ crystals, the thermal conductivity of crystals declines. The temperature dependence of thermal conductivity after annealing changes in the same way as for 8Sc0.5Ce0.5YSZ, i. e. the steepness of $k(T)$ curve rises and thermal conductivity increases at 300 K after annealing. However, with higher total concentration of the co-doping oxides in crystals, the difference in thermal conductivity before and after annealing decreases (Figure 5, Table 3).

Thus, we may say that annealing has different impact on thermal conductivity of ScCeSZ and ScCeYSZ crystals. In case of ScCeSZ compounds, with the appearance of a rhombohedral phase, thermal conductivity declines in the temperature range 50–200 K, and then in the range 200–300 K, thermal conductivity approaches its values before annealing. As a result of annealing, the content of the tetragonal phase in ScCeYSZ crystals goes up, and when the temperature rises to a room temperature thermal conductivity increases, exceeding its pre-annealing values. As a result of annealing, no rhombohedral phase was observed in the studied ScCeYSZ specimens, but only

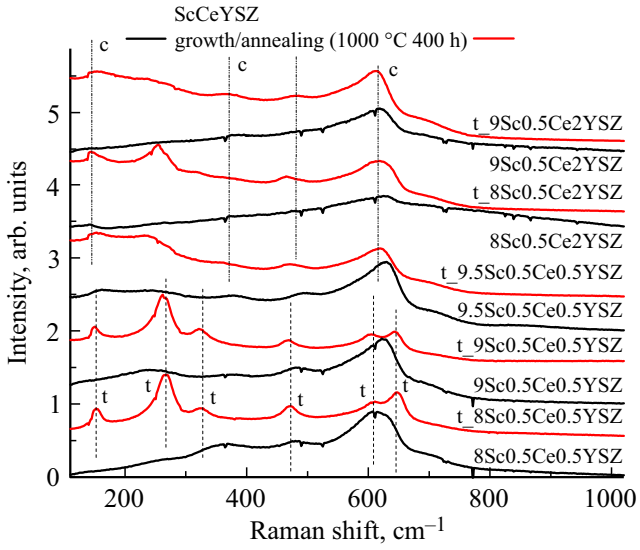

Figure 5. RS spectra of ScCeYSZ crystals before and after annealing at a temperature of 1000 °C during 400 h.

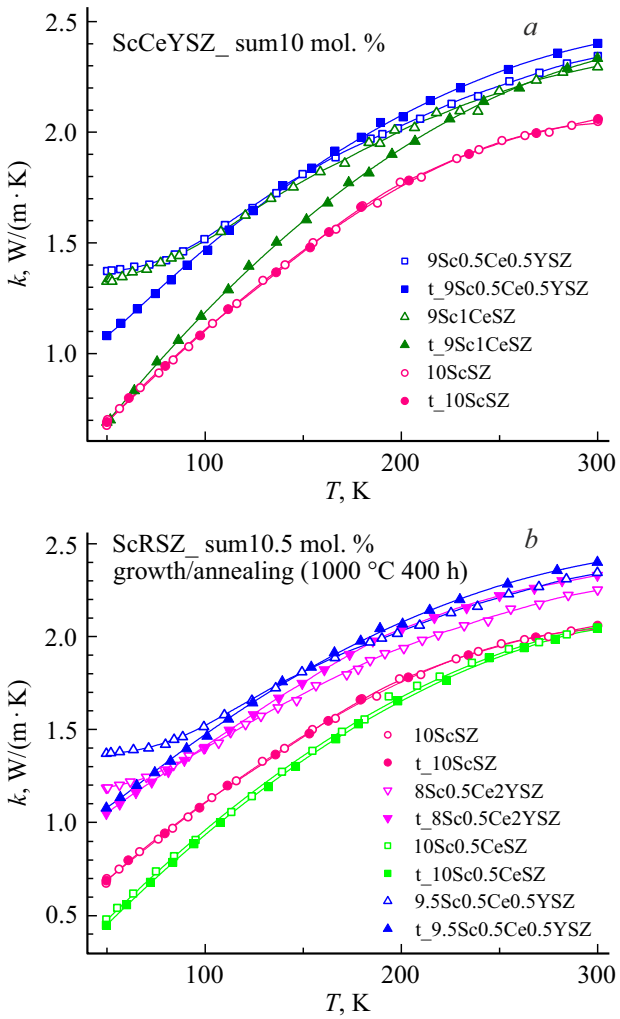

Figure 6. Temperature dependences of thermal conductivity before and after annealing at the same total concentrations of the doping impurities, compared: *a*) 10 mol.%; *b*) 10.5 mol.%.

an increase in the tetragonal phase and/or local regions with the ordering of oxygen vacancies in 8Sc0.5Ce0.5YSZ, 9Sc0.5Ce0.5YSZ and 9.5Sc0.5Ce0.5YSZ. As a result of these structural changes, the steepness of the temperature curve

$k(T)$ and the absolute values of thermal conductivity k grow up. This trend of thermal conductivity variation is most noticeable after annealing in 8Sc0.5Ce0.5YSZ crystals. With an increase in the total concentration of the doping impurity, the amount of change in thermal conductivity during annealing becomes lower.

Figure 6 illustrates comparison of temperature dependences of thermal conductivity before and after annealing of ScSZ [31], ScCeSZ and ScCeYSZ crystals under the same total concentrations of doping impurities 10 mol.% (Figure 6, *a*) and 10.5 mol.% (Figure 6, *b*).

It is clearly seen that with a total content of doping impurities of 10 mol.% (Figure 6, *a*), 10ScSZ crystals have the lowest thermal conductivity, which practically does not change during annealing. Introduction of CeO_2 and Y_2O_3 slightly enhances thermal conductivity of crystals. After annealing of ScCeSZ specimens in the temperature range of 50−100 K, it sharply decreases to the level of thermal conductivity of 10ScSZ crystals. In case of ScCeYSZ crystals, the changes in thermal conductivity in the low-temperature region are significantly smaller, and when the temperature rises to room temperature, it becomes slightly higher than its values before annealing.

With a doping impurity content of 10.5 mol.% (Figure 6, *b*), 10Sc0.5CeSZ crystals exhibit a lower thermal conductivity than 10ScSZ due to a higher content of impurities with almost the same phase composition [31]. Thermal conductivity of 10Sc0.5CeSZ, crystals, similar to 10ScSZ, remained practically unchanged in annealing. It should be emphasized that the degree of change of thermal conductivity in 8Sc0.5Ce2YSZ and 9.5Sc0.5Ce0.5YSZ crystals (Figure 6, *b*) after annealing is less than in 9Sc0.5Ce0.5YSZ and 9Sc1CeSZ with a total content of the doping impurity of 10 mol.% (Figure 6, *a*).

4. Conclusion

The effect of heat treatment at 1000 °C for 400 h on thermal conductivity of crystals stabilized with scandium and cerium oxides $(ZrO_2)_{1-x-y}(Sc_2O_3)_x(CeO_2)_y$, where $x = 0.08-0.1$, $y = 0.005-0.01$, and at the same time stabilized with scandium, cerium and yttrium oxides $(ZrO_2)_{1-x-y-z}(Sc_2O_3)_x(CeO_2)_y(Y_2O_3)_z$, where $x = 0.08-0.1$, $y = 0.005-0.01$, $z = 0.005-0.02$ was studied.

It is shown that a prolonged annealing (400 h) at a temperature of 1000 °C on crystals doped with scandium and cerium oxides $(ZrO_2)_{1-x-y}(Sc_2O_3)_x(CeO_2)_y$, where $x = 0.08-0.1$, $y = 0.005-0.01$, can lead to phase instability of solid solutions and a corresponding change in thermal conductivity depending on their composition. In case of 8.5Sc0.5CeSZ, 9Sc1CeSZ, 9.5Sc0.5CeSZ crystals the appearance of local regions with structures similar to those of the rhombohedral and tetragonal phases in solid solutions as a result of the ordering of oxygen vacancies causes a change in thermal conductivity at low temperatures (50−100 K). A more noticeable increase in the rhombohedral phase content in 9.5Sc0.5CeSZ crystals after annealing leads to a lower thermal conductivity at a room temperature as well. The presence of rhombohedral and cubic phases in 10Sc0.5CeSZ crystals before and after annealing demonstrates poor annealing effect on thermal conductivity and maintains its minimum (among other compositions) values.

The study of crystals doped with scandium, cerium, and yttrium oxides $(ZrO_2)_{1-x-y-z}(Sc_2O_3)_x(CeO_2)_y(Y_2O_3)_z$, where $x=0.08-0.1$, $y = 0.005-0.01$, $z = 0.005-0.02$, has shown that the addition of yttrium to the stabilizing composition increases phase stability and reduces the effect of annealing on thermal conductivity. When annealing ScCeSZ crystals, the low-temperature thermal conductivity decreases with the appearance of a rhombohedral phase. As a result of annealing, no rhombohedral phase was observed in ScCeYSZ crystals, but only an increase in the tetragonal phase and/or local regions with the ordering of oxygen vacancies. As a result of these structural changes, the slope of the $k(T)$ curve and the absolute values of thermal conductivity in ScCeYSZ crystals increase. To the highest extent it was observed for 8Sc0.5Ce0.5YSZ. With the rise of total concentration of doping impurities the effect of annealing on thermal conductivity was noticed to decline.

Funding

The study was financially supported by the Ministry of Science and Higher Education of the Russian Federation (scientific topic code FZRS-2025-0001) and was made under the state assignment of the Federal State Budgetary Institution of Higher Education „National Research Mordovian State University named after N.P. Ogarev“ using equipment from the Collective Use Centers of the Federal Research Center „Institute of General Physics named after A.M. Prokhorov of the Russian Academy of Sciences and Bryansk State University named after I.G. Petrovsky.

Conflict of interest

The authors declare that they have no conflict of interest.

References

[1] J. Chevalier, A. Liens, H. Reveron, F. Zhang, P. Reynaud, T. Douillard, L. Preiss, V. Sergo, V. Lughi, M. Swain, N. Courtois. J. Am. Ceram. Soc. **103**, *3*, 1482 (2020).
[2] M. Sabzi, S.M. Dezfuli, Z. Balak. Int. J. Min. Met. Mater. **26**, *8*, 1020 (2019).
[3] F. Kazemi, F. Arianpour, M. Taheri, A. Saberi, H.R. Rezaie. Int. J. Min. Met. Mater. **27**, *5*, 693 (2020).
[4] E. Peng, X. Wei, U. Garbe, D. Yu, B. Edouard, A. Liu, J. Ding. J. Mater. Sci. **53**, *1*, 247 (2018).
[5] Q. Li, X. Hao, Y. Gui, H. Qiu, Y. Ling, H. Zheng, M. Omran, L. Gao, J. Chen, G. Chen. Ceram. Int. **47**, *19*, 27188 (2021).
[6] C. Piconi, G. Maccauro. Biomater. **20**, *1*, 1 (1999).
[7] R.H.J. Hannink, P.M. Kelly, B.C. Muddle. J. Am. Ceram. Soc. **83**, *3*, 461 (2000).

[8] J. Chevalier, L. Gremillard, A.V. Virkar, D.R. Clarke. J. Am. Ceram. Soc. **92**, *9*, 1901 (2009).
[9] B. Basu, J. Vleugels, O. Van Der Biest. J. Eur. Ceram. Soc. **24**, *7*, 2031 (2004).
[10] M. Yashima, M. Kakihana, M. Yoshimura. Solid State Ionics **86–88**, *Part 2*, 1131 (1996).
[11] Y. Suzuki. Solid State Ionics **81**, *3–4*, 211 (1995).
[12] T. Götsch, W. Wallisch, M. Stöger-Pollach, B. Klötzer, S. Penner. AIP Advances **6**, *2*, 025119 (2016).
[13] M. Chen, B. Hallstedt, L.J. Gauckler. Solid State Ionics **170**, *3–4*, 255 (2004).
[14] E.R. Andrievskaya. J. Eur. Ceram. Soc. **28**, *12*, 2363 (2008).
[15] C. Wang. PhD Thesis. Max-Planck-Institut für Metallforschung, Stuttgart (2006). 169 p.
[16] N.R. Rebollo, A.S. Gandhi, C.G. Levi. In: High Temperature Corrosion and Materials Chemistry IV / Eds E. Opila, P. Hou, T. Maruyama, B. Pieraggi, E. Wuchina. Electrochem. Soc. Proc. **PV-2003-16**, 431 (2003).
[17] L. Li, O. Van der Biest, S.-G. Huang, J. Vleugels, P.-L. Wang. J. Shanghai Univ. (English Edition), **10**, *1*, 65 (2006).
[18] R. Ruh, H.J. Garrett, R.F. Domagala, V.A. Patel. J. Am. Ceram. Soc. *60*, *9–10*, 399 (1977).
[19] T.-S. Sheu, J. Xu, T.-Y. Tien. J. Am. Ceram. Soc. **76**, *8*, 2027 (1993).
[20] M. Bahamirian, S.M.M. Hadavi, M.R. Rahimipour, M. Farvizi, A. Keyvani. Metall. Mater. Trans. A **49**, *6*, 2523 (2018).
[21] K. Bobzin, L. Zhao, M. Öte, T. Königstein. Surf. Coatings Technol. **366**, 349 (2019).
[22] X. Wei, G. Hou, Y. An, P. Yang, X. Zhao, H. Zhou, J. Chen. Ceram. Int. **47**, *5*, 6875 (2021).
[23] S. Lawson. J. Eur. Ceram. Soc. **15**, *6*, 485 (1995).
[24] C. Pecharromán, J.F. Bartolomé, J. Requena, J.S. Moya, S. Deville, J. Chevalier, G. Fantozzi, R. Torrecillas. Adv. Mater. **15**, *6*, 507 (2003).
[25] S.P.S. Badwal. Solid State Ionics **143**, *1*, 39 (2001).
[26] W. Araki, T. Koshikawa, A. Yamaji, T. Adachi. Solid State Ionics **180**, *28–31*, 1484 (2009).
[27] G. Di Girolamo, C. Blasi, M. Schioppa, L. Tapfer. Ceram. Int. **36**, *3*, 961 (2010).
[28] H. Liu, S. Li, Q. Li, Y. Li. Mater. Design **31**, *6*, 2972 (2010).
[29] D.A. Agarkov, M.A. Borik, V.T. Bublik, A.S. Chislov, A.V. Kulebyakin, I.E. Kuritsyna, V.A. Kolotygin, E.E. Lomonova, F.O. Milovich, V.A. Myzina, V.V. Osiko, N.Yu. Tabachkova. J. Alloy. Compd. **791**, 445 (2019).
[30] D.A. Agarkov, M.A. Borik, G.M. Korableva, A.V. Kulebyakin, I.E. Kuritsyna, E.E. Lomonova, F.O. Milovich, V.A. Myzina, P.A. Popov, P.A. Ryabochkina, N.Yu. Tabachkova. Phys. Solid State **62**, *12*, 2357 (2020).
[31] Q.-L. Li, X.-Z. Cui, S.-Q. Li, W.-H. Yang, C. Wang, Q. Cao. J. Therm. Spray Technol. **24**, *1–2*, 136 (2015).
[32] L. Sun, H. Guo, H. Peng, S. Gong, H. Xu. Progr. Natur. Sci. **23**, *4*, 440 (2013).
[33] S. Raghavan, H. Wang, W.D. Porter, R.B. Dinwiddie, M.J. Mayo. Acta Materialia **49**, *1*, 169 (2001).
[34] Z.Z. Wang, Y. Bai, W. Fan, Y. Gao, Q. Liu, R.J. Wang, W.Z. Tao, F. Ma. Comput. Mater. Sci. **174**, 109478 (2020).
[35] W. Fan, Y. Bai, Z.Z. Wang, J.W. Che, Y. Wang, W.Z. Tao, R.J. Wang, G.Y. Liang. J. Eur. Ceram. Soc. **39**, *7*, 2389 (2019).
[36] W. Fan, Z.Z. Wang, Y. Bai, J.W. Che, R.J. Wang, F. Ma, W.Z. Tao, G.Y. Liang. J. Eur. Ceram. Soc. **38**, *13*, 4502 (2018).
[37] F. Yang, X. Zhao, P. Xiao. Acta Materialia **60**, *3*, 914 (2012).
[38] X. Huang, D. Wang, M. Lamontagne, C. Moreau. Mater. Sci. Eng. B **149**, *1*, 63 (2008).
[39] R. Ahmadi-Pidani, R. Shoja-Razavi, R. Mozafarinia, H. Jamali. Ceram. Int. **38**, *8*, 6613 (2012).
[40] M.A. Borik, A.V. Kulebyakin, I.E. Kuritsyna, E.E. Lomonova, P.A. Popov, V.A. Myzina, F.O. Milovich, N.Yu. Tabachkova. Phys. Solid State **61**, *12*, 2397 (2019).
[41] P.A. Popov, A.A. Sidorov, E.A. Kulchenkov, A.M. Anishchenko, I.C. Avetissov, N.I. Sorokin, P.P. Fedorov. Ionics **23**, *1*, 233 (2017).
[42] M.A. Borik, R.M. Eremina, E.E. Lomonova, V.A. Myzina, V.V. Osiko, I.I. Fazlizhanov, V.A. Shustov, I.V. Yatsyk. Modern Electron. Mater. **3**, *3*, 95 (2017).
[43] D. Agarkov, M. Borik, G. Eliseeva, A. Kulebyakin, E. Lomonova, F. Milovich, V. Myzina, Y. Parkhomenko, E. Skryleva, N. Tabachkova. Crystals **10**, *1*, 49 (2020).
[44] V.M. Orera, R.I. Merino, F. Peñ a. Solid State Ionics **72**, *2*, 224 (1994).
[45] P.A. Popov, P.P. Fedorov, V.A. Konyushkin, A.N. Nakladov, S.C. Kuznetsov, V.V. Osiko, T.T. Basiev. Dokl. RAN **421**, *5*, 614 (2008) (in Russian).
[46] M. Févre, A. Finel, R. Caudron, R. Mévrel. Phys. Rev. B **72**, *10*, 104118 (2005).
[47] D.A. Agarkov, M.A. Borik, V.T. Bublik, S.I. Bredikhin, A.S. Chislov, A.V. Kulebyakin, I.E. Kuritsyna, E.E. Lomonova, F.O. Milovich, V.A. Myzina, V.V. Osiko, N.Yu. Tabachkova. Solid State Ionics **322**, 24 (2018).
[48] M.A. Borik, A.S. Chislov, A.V. Kulebyakin, I.E. Kuritsyna, V.A. Kolotygin, E.E. Lomonova, F.O. Milovich, V.A. Myzina, N.Yu. Tabachkova. Data in Brief **25**, 104061 (2019).
[49] D.A. Agarkov, M.A. Borik, S.I. Bredikhin, I.N. Burmistrov, G.M. Eliseeva, V.A. Kolotygin, A.V. Kulebyakin, I.E. Kuritsyna, E.E. Lomonova, F.O. Milovich, V.A. Myzina, P.A. Ryabochkina, N.Yu. Tabachkova, T.V. Volkova. J. Materiomics **5**, *2*, 273 (2019).
[50] H. Fujimori, M. Yashima, M. Kakihana, M. Yoshimura. J. Am. Ceram. Soc. **81**, *11*, 2885 (1998).

Translated by T.Zorina